JACS
JOURNAL OF THE AMERICAN CHEMICAL SOCIETY

Article

pubs.acs.org/JACS

Polarized XANES Monitors Femtosecond Structural Evolution of Photoexcited Vitamin B_{12}

Nicholas A. Miller,[†] Aniruddha Deb,[†,§] Roberto Alonso-Mori,[∥] Brady D. Garabato,[⊥] James M. Glownia,[∥] Laura M. Kiefer,[†] Jake Koralek,[∥] Marcin Sikorski,[∥] Kenneth G. Spears,[†] Theodore E. Wiley,[†] Diling Zhu,[∥] Pawel M. Kozlowski,[⊥,#,¶] Kevin J. Kubarych,[†,§] James E. Penner-Hahn,[†,§] and Roseanne J. Sension*[,†,‡,§]

[†]Department of Chemistry, University of Michigan, 930 N University Avenue, Ann Arbor, Michigan 48109-1055, United States
[‡]Department of Physics, University of Michigan, 450 Church Street, Ann Arbor, Michigan 48109-1040, United States
[§]Biophysics, University of Michigan, 930 N University Avenue, Ann Arbor, Michigan 48109-1055, United States
[∥]Linac Coherent Light Source, SLAC National Accelerator Laboratory, 2575 Sand Hill Road, Menlo Park, California 94025, United States,
[⊥]Department of Chemistry, University of Louisville, 2320 South Brook Street, Louisville, Kentucky 40292, United States
[#]Department of Food Sciences, Medical University of Gdansk, Al. Gen J. Hallera 107, 80-416 Gdansk, Poland

Supporting Information

ABSTRACT: Ultrafast, polarization-selective time-resolved X-ray absorption near-edge structure (XANES) was used to characterize the photochemistry of vitamin B_{12}, cyanocobalamin (CNCbl), in solution. Cobalamins are important biological cofactors involved in methyl transfer, radical rearrangement, and light-activated gene regulation, while also holding promise as light-activated agents for spatiotemporal controlled delivery of therapeutics. We introduce polarized femtosecond XANES, combined with UV−visible spectroscopy, to reveal sequential structural evolution of CNCbl in the excited electronic state. Femtosecond polarized XANES provides the crucial structural dynamics link between computed potential energy surfaces and optical transient absorption spectroscopy. Polarization selectivity can be used to uniquely identify electronic contributions and structural changes, even in isotropic samples when well-defined electronic transitions are excited. Our XANES measurements reveal that the structural changes upon photoexcitation occur mainly in the axial direction, where elongation of the axial Co−CN bond and Co−N_{Im} bond on a 110 fs time scale is followed by corrin ring relaxation on a 260 fs time scale. These observations expose features of the potential energy surfaces controlling cobalamin reactivity and deactivation.

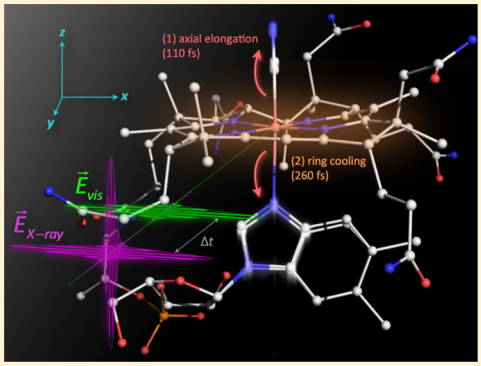

INTRODUCTION

Light is a versatile energy source that can be shaped, timed, tuned, focused, aimed, and delivered to a target, permitting spatial and temporal control of molecular scale devices. At the heart of this exquisite control is photochemistry, where photon energy is transduced into action by the movement of charge, change in shape, or cleavage of a bond. Understanding and optimizing the reactivity both of natural photoreceptors and synthetic light-activated delivery agents requires detailed characterization of the photochemical reaction mechanism, ideally by observing the electronic and structural transformations as they occur.

Many important photoreceptors involve metal centers, often with cyclic tetrapyrrole ligands. Chlorins are active in light harvesting and electron transfer in photosynthetic systems. Natural and synthetic metalloporphyrins are used in energy conversion, medical therapeutics, photodynamic therapy, molecular electronics, spintronics, signaling, and sensors.[1] Biological functions for cobalamins (vitamin B_{12} cofactors) include light-activated gene regulation triggered through photolysis of the Co−C bond.[2−5] Synthetic cobalamins are finding increasing use as light-activated agents for controlled spatiotemporal delivery of therapeutic agents.[6] In the spirit of optical modulation of biological function, a new generation of targeted therapeutics would be enabled by the development of a biocompatible and flexibly configurable molecular scaffold whose function can be placed entirely under optical control. Cobalamins have the potential to serve as a foundation for such a platform by leveraging their extensive and well-characterized biochemical pathways and transport machinery.

With the very recent development of X-ray free electron laser (XFEL)-based time-resolved X-ray absorption spectroscopy (XAS), it is now possible to interrogate directly the local

Received: October 30, 2016
Published: January 30, 2017

DOI: 10.1021/jacs.6b11295
J. Am. Chem. Soc. 2017, 139, 1894−1899

electronic and structural changes that take place around the central metal atom of inorganic photoreceptors at the earliest stages of photochemical excitation.[7−11] Here, we add a key experimental degree of freedom, polarization, that has long been leveraged in optical spectroscopy but which has yet to be applied to transient XAS on femtosecond time scales. Polarization control adds an important element to the toolkit. While X-ray absorption near-edge structure (XANES) spectra are generally underdetermined, making it difficult to uniquely determine bond lengths and angles from XANES data alone, it is possible to assign qualitative changes based on these data. Polarization-resolved changes can be used to uniquely identify electronic contributions and structural changes, even in isotropic samples when well-defined electronic transitions are excited.

We report the use of femtosecond XAS at the Co K-edge to characterize the photochemistry of vitamin B_{12} (CNCbl or cyanocobalamin) in solution. CNCbl is an ideal molecule for initial femtosecond XAS studies because it undergoes a large geometry change upon optical excitation, the quantum yield for return to the ground state approaches unity, and the excited-state geometries sampled are relevant to reactive coordinates in photolabile cobalamins.[12−14] The optically allowed states in the visible and near-UV region of the spectrum involve $\pi\pi^*$ transitions of the corrin ring.[13−20] Excitation at 550 nm initially populates a $\pi^1\pi^{*1}$ state followed by rapid increase in d-electron character to a $\pi^1(d_{xy}+n/\pi^*)^1$ configuration.[14,19] Subsequent internal conversion to a $\pi^1(\sigma^*d_{z^2})^1$ configuration results in the stable S_1 excited state molecule.[14]

Cobalt XANES is sensitive to the position and identity of the nearest neighbors to the cobalt. Thus, time-resolved XANES provides direct information on the ligation changes that take place following optical excitation. The excitation pulse preferentially selects those molecules with transition dipole components along the direction of the laser polarization. Similarly, X-ray absorption preferentially samples the structure in the direction of the X-ray polarization. By adjusting the relative polarizations of the visible pump and the X-ray probe pulses, it is possible to separate the direction-dependent components for isotropic solutions, revealing excited-state structural dynamics around the cobalt. Our data provide direct evidence for a sequential mechanism (Figure 1) in which the initial excitation of the corrin ring $\pi\pi^*$ transition results in small changes in the Co ligation followed by delayed elongation of the axial Co−cyanide (Co−CN) and Co−dimethylbenzimidazole ($Co-N_{Im}$) bonds on a 110 fs time scale. Additional relaxation of the equatorial ligand follows on a 260 fs time scale.

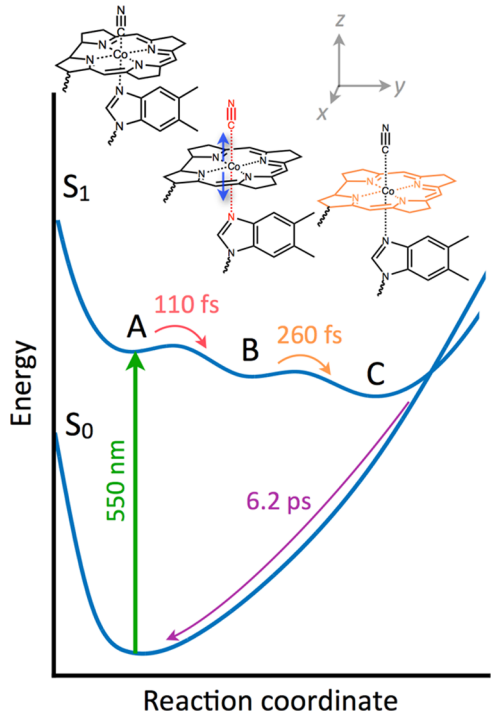

Figure 1. Cartoon potential energy diagram summarizes the structural changes induced by 550 nm excitation to the lowest optically allowed excited state. The molecule fixed coordinate system is also indicated. Time scales obtained with transient XAS match those of visible transient absorption, providing a consistent picture of the dynamics but adding the crucial missing dynamical information for the cobalt ligands.

EXPERIMENTAL METHODS

Polarized XANES difference spectra were obtained for time delays between −0.15 and 2 ps using the XPP instrument of the XFEL LCLS at SLAC.[21] The optical pump pulse (~50 fs full width at half-maximum (fwhm)) was centered at 550 nm near the peak of the lowest-energy optical transition (see Figure S1 for a UV−visible spectrum of CNCbl). The X-ray probe pulse (~40 fs fwhm) was tuned from 7.7 to 7.8 keV, and cobalt X-ray fluorescence was collected as a measure of X-ray absorption. The effective instrument response function, determined by the convolution of the optical laser with the X-ray laser, was ~70 fs. The jitter of X-ray/laser synchronization was recorded and used to obtain time-resolved XANES spectra for parallel and perpendicular polarization for time delays from −150 to 700 fs.[21,22] The data were averaged using 50 fs bins centered every 25 fs.

The CNCbl sample was dissolved in ultrapure deionized water to a concentration of 8.8 mM and pumped through a glass nozzle to achieve a stable 50 μm diameter jet of solution. The polarization of the optical laser was rotated to be parallel or perpendicular to the polarization of the X-ray laser. The measured XANES spectrum with the optical laser off is in excellent agreement with the spectrum reported by Champloy et al. for CNCbl free of radiation damage.[23] The use of femtosecond X-ray pulses with a large circulating sample volume avoids the complication of radiation damage. The dark-state XANES spectra were compared and found to be identical throughout each run. The measured signal as a function of laser power was used to estimate the percent of the sample excited by the optical pulse. For the measurements reported here, approximately 20% of the molecules in the sample volume were excited. Details of this estimate are provided in the Supporting Information.

UV−visible transient absorption measurements with 550 nm excitation and a broadband continuum probe spanning the range from 280 to 600 nm were performed for comparison with the XANES measurements. The continuum was generated by focusing the 400 nm second harmonic of a Ti:sapphire laser into a translating CaF_2 window as described previously.[12,24] The sample was a flat wire-guided flow of a 0.43 mM solution of CNCbl in water. All measurements were performed with a magic angle orientation of the pump and probe polarization (54.7°) to produce an isotropic transient absorption signal. The results of the transient absorption measurements are described in detail in the Supporting Information.

RESULTS AND DISCUSSION

Polarized XANES difference spectra, $\Delta S_{\parallel/\perp} = S_{\text{Laser on}} - S_{\text{Laser off}}$, were obtained for time delays between −0.15 and 0.7 ps, at 1.5 ps, and at 2 ps. Difference spectra for select time delays between 45 fs and 1.5 ps are plotted in Figure 2.

The isotropic difference spectra (Figure 3a) may be calculated from the polarized measurements as $\Delta S_{\text{isotropic}} = \Delta S_{\parallel} + 2\Delta S_{\perp}$. The transition dipole excited at 550 nm is in the plane of the corrin ring.[16,17] In what follows, this direction is designated x; the orthogonal in-plane direction is y, and the z-direction is out of the

DOI: 10.1021/jacs.6b11295
J. Am. Chem. Soc. 2017, 139, 1894−1899

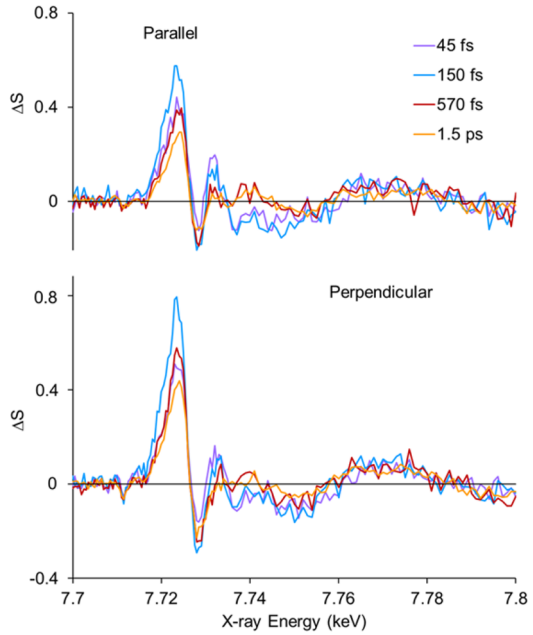

Figure 2. Polarized XANES difference spectra in four representative time regions.

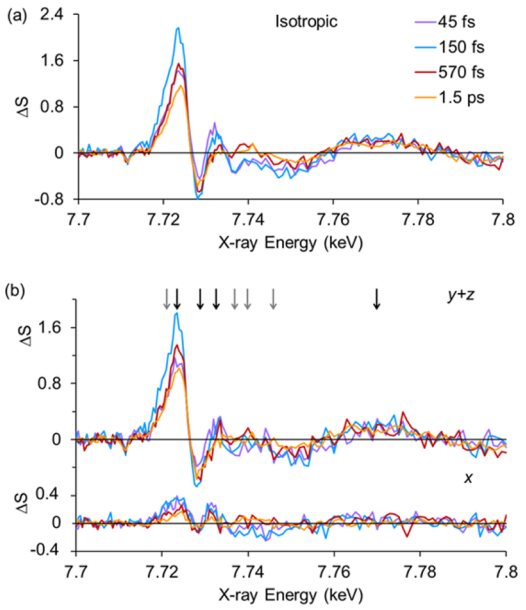

Figure 3. Time-dependent XAS. (a) Isotropic XANES difference spectra derived from the polarization data in Figure 2. (b) XANES difference spectra in the x and $y + z$ directions derived from the polarization data. The black arrows indicate energies for which time kinetics are analyzed in Figure 4. Analysis at the energies indicated by the gray arrows is included in Supporting Information Figure S10.

plane of the corrin ring. Since rotational diffusion of CNCbl is much longer than the lifetime of the excited state, the orientation of the molecule is effectively fixed in space during these measurements.[25] The measured signals $\Delta S_{\parallel}$ and $\Delta S_{\perp}$ can be used to extract the ΔS_x and ΔS_{y+z} contributions parallel and perpendicular to the optical transition dipole.[26]

$$\left.\begin{aligned}\Delta S_{\parallel} &= 0.6\Delta S_x + 0.2\Delta S_y + 0.2\Delta S_z\\ \Delta S_{\perp} &= 0.2\Delta S_x + 0.4\Delta S_y + 0.4\Delta S_z\end{aligned}\right\} \Rightarrow \begin{aligned}\Delta S_x &= 2\Delta S_{\parallel} - \Delta S_{\perp}\\ \Delta S_{y+z} &= 3\Delta S_{\perp} - \Delta S_{\parallel}\end{aligned}$$

These contributions are plotted in Figure 3b.

Qualitatively, the polarized XANES difference spectra show large changes in $y + z$ and only small changes in x. Although y-polarized spectra were not observed directly in this experiment, the corrin ring geometry requires that x- and y-polarized signals be similar in magnitude. The experimental results thus demonstrate unequivocally that photoexcitation predominantly affects the axial bond lengths along the z-direction.

Analysis of the time evolution reveals new intermediates as CNCbl relaxes to the stable excited-state minimum. The x and $y + z$ traces at eight X-ray energies were fit to a model consisting of a sum of exponential decay components. The longest time constant was set at 6.2 ps, corresponding to the overall decay of the excited-state population (see below and Supporting Information Figure S8). The other two time constants were allowed to vary, resulting in $\tau_A = 0.12 \pm 0.03$ ps and $\tau_B \approx 0.3 \pm 0.1$ ps. Fits at key X-ray energies are plotted in Figure 4 (see also Supporting Information Figure S10).

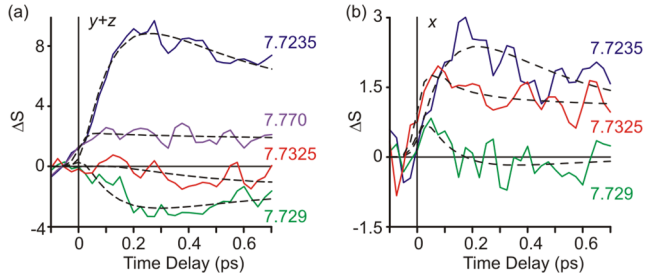

Figure 4. (a) Time traces for the $y + z$ difference signal at select X-ray energies. Black dashed lines are exponential fits to the data as described in the text. (b) Time traces for the x difference signal at select X-ray energies.

Very similar time constants were obtained for UV−visible transient absorption measurements following 550 nm excitation. These data were fit to a sum of exponential decay components resulting in three unique species having lifetimes of $\tau_A = 0.11 \pm 0.03$ ps, $\tau_B = 0.26$ ps ± 0.03 ps, and $\tau_C = 6.2 \pm 0.1$ ps (Figure 5a and Supporting Information Figures S4−S7). The 6.2 ps decay of the excited-state population is in good agreement with earlier measurements.[27−30]

Assuming a sequential model, ground state (GS) $\xrightarrow{h\nu}$ intermediate A (lifetime 0.11 ps) → intermediate B (lifetime 0.26 ps) → intermediate C (lifetime 6.2 ps) → GS (see Figure 1), the amplitudes of the decay components can be used to estimate species associated difference spectra for the short-lived states in both the UV−visible and XANES regions of the spectrum (Figure 5b,c). Details of the analysis are provided in the Supporting Information. The XANES difference spectrum for the initial intermediate here designated "A" has a small amplitude with comparable magnitude for both x and $y + z$ components, consistent with $(\pi^2 \rightarrow \pi^1\pi^{*1})$ excitation of the corrin ring resulting in modest changes in the equatorial ligation of the cobalt. The UV−visible difference spectrum is characterized by small changes across the spectrum. Time-dependent density functional theory (TD-DFT) calculations indicate that the initial intermediate A $(\pi^1(\pi^*/d_{xy}+n^*)^1)$ following optical excitation has d-orbital character that increases with structural relaxation along the electronic excited-state surface prior to changes in axial bond length. The B $(\pi^1(\sigma^*d_{z^2})^1)$ intermediate formed on a ca. 0.11 ps time scale is characterized by a large increase in the $y + z$ XANES

DOI: 10.1021/jacs.6b11295
J. Am. Chem. Soc. 2017, 139, 1894−1899

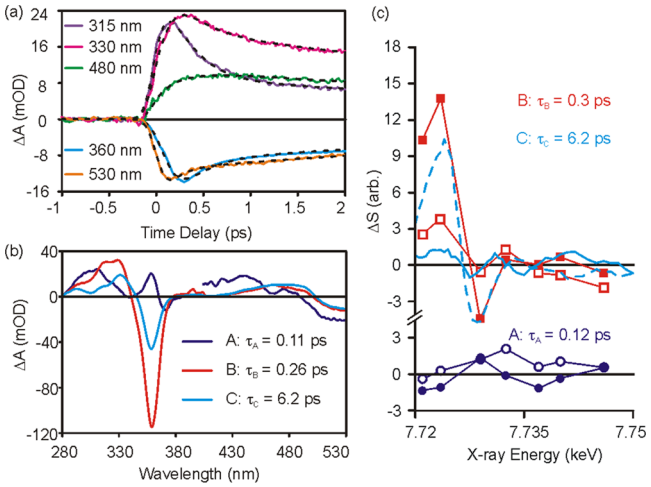

Figure 5. Species associated difference spectra (SADS). (a) UV−visible time traces at select wavelengths, as indicated. The 360 nm trace is divided by 5 to fit on the same scale. The black dashed lines represent the fit to the data. (b) SADS for the three intermediates contributing to the excited-state absorption signal. (c) Estimated SADS for the x (open symbols) and $y + z$ (filled symbols) components of the XANES difference spectrum of the initial excited-state intermediate (A, dark blue circles) and the first hot intermediate state (B, red squares) constructed from the amplitudes of the decay components. Spectra for A and B are offset vertically. The difference amplitude for intermediate C (light blue lines, measured at 1.5 ps) is overlaid on the same scale as B. The solid line is x, and the dashed line is $y + z$.

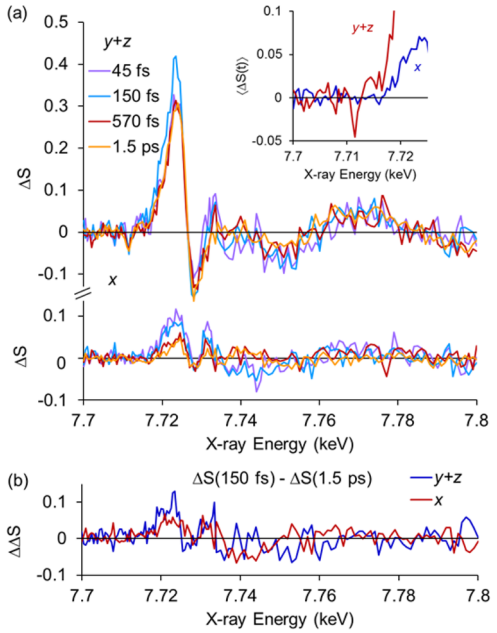

Figure 6. XANES difference spectra at four time delays following optical excitation. (a) Contributions of $y + z$ and x to the difference spectra. The magnitude of each spectrum has been scaled to constant population using the 6.2 ps lifetime of the excited state. The 45 fs spectrum is also corrected for the instrument-limited rise of the population. The unscaled data are plotted in Figure 3b. The inset illustrates the time-averaged difference in the pre-edge region. (b) Magnitude of the change in the spectrum between 150 fs and 1.5 ps for both the x and $y + z$ components.

difference signal, consistent with axial antibonding character resulting in elongation of axial bonds. The UV−visible spectrum is characterized by a large decrease in the γ-band intensity at 361 nm, a spectral region sensitive to the oxidation state and axial ligation of the cobalt.[15]

As the molecule relaxes to the excited-state minimum, intermediate C ($(\pi^1(\sigma^*d_{z^2})^1)$, on a ca. 0.26 ps time scale, there is a decrease in the difference signal at the XANES edge at 7.23 keV, a change in the structure between 7.73 and 7.75 keV as shown in Figure 3a, and a decrease in the magnitude of the bleach at 361 nm (Figure 5b) indicating an increase in the intensity of the γ-band in the UV−visible spectrum. Although we have assigned both states B and C to nominal $(\pi^1(\sigma^*d_{z^2})^1)$ electronic configurations because of the axial elongation deduced from the XANES difference spectra for both states, the large change in the UV absorption spectrum from B to C suggests that this transition is not simply vibrational relaxation. There is an accompanying change in the electronic character of the excited state.

To compare the XANES difference spectra of the excited states, we have normalized the data plotted in Figure 3b to constant population, accounting for the instrument-limited rise of population in the 45 fs spectrum and the overall exponential decay of the excited-state population on a 6.2 ps time scale at all time delays. The observed changes between the excited states B and C are of similar magnitude in both the x and $y + z$ contributions (Figure 6a). This is illustrated most clearly in Figure 6b, where the difference between the signal measured at 150 fs (~50% B and 25% each A and C) and 1.5 ps (99+% C) is plotted for both contributions. This comparison demonstrates that the spectral change is predominantly in x and y, suggesting that the dominant structural change occurring on the 0.26 ps time scale involves corrin ring relaxation. Finally, the bleach of the 1s → 3d pre-edge absorption in intermediates B and C (inset to Figure 6a) is limited to the $y + z$ component, consistent with the expected population of a $3d_{z^2}$ orbital in the excited state decreasing the intensity of the 1s → $3d_{z^2}$ transition.

Comparison with Simulations. The photochemistry of cobalamins is controlled by several low-lying excited states. The lowest S_1 potential energy surface results from the interaction of these states.[13,14,18−20,31] Theoretical simulations show that the relative energies of the different excited states are most sensitive to the changes in axial bond lengths, while distortion of the corrin ring is important as an effective channel for deactivation.[31] Pump−probe transient absorption spectra in the UV−visible and IR regions are consistent with these conclusions but provide only indirect information on structural changes.[1,27−30,32−36] Comparison of the measured XANES spectra of the relaxed excited-state intermediate C with XANES spectra predicted for the calculated excited-state structure provides additional insight into the excited-state dynamics.

The excited states of CNCbl were calculated using the TD-DFT framework and a truncated model system for cobalamin.[14,18−20] These calculations predict that excitation at 550 nm will result in the formation of an electronic state, C in Figure 1, characterized by a substantial increase of axial bond lengths from (Co−CN, Co−N_{Im}) = (185.7 pm, 205.4 pm) in the ground state to (221.6 pm, 227.5 pm) in the excited state and a change in the Co−C≡N bond angle from 179 to 170°.[14] These structural parameters were used to simulate the polarized XANES for the relaxed S_1 state structure.

The Co K-edge XANES simulations were performed by using the FDMNES ab initio code.[37,38] Within FDMNES, a full potential finite difference method was used to solve the Schrödinger equation in order to permit the use of non-muffin-tin potentials. A Hedin−Lundqvist potential was used for

DOI: 10.1021/jacs.6b11295
J. Am. Chem. Soc. 2017, 139, 1894−1899

the exchange correlation, and the spectra were convoluted using a Lorentzian function with a constant broadening to simulate the core level width, which was determined by the program, and an additional energy-dependent broadening to account for the final state width using an arctangent formula.[38]

Theoretical calculations place the transition dipole for the absorption at 550 nm along the direction defined approximately by the methylene groups on opposite sides of the corrin ring (Figure 1).[14,17,19] Thus, the in-plane direction designated "x" is expected to correspond to this axis. The y-direction is orthogonal to x in the plane of the corrin ring, while z is the orthogonal out-of-plane direction along the Co−C≡N bond. This coordinate system was used in the simulations. Continuum transitions above the Fermi energy excite a photoelectron from the 1s orbital. This photoelectron propagates as a p-symmetric wave oriented in the direction of the polarization vector of the X-ray. Structural features contribute to the difference spectrum with a weight of $\cos^2\theta$, where θ is the angle between a structural feature and the polarization axis.[39,40] This is incorporated into the simulation program. The isotropic spectrum is the sum of the x, y, and z contributions.

Simulations performed for the truncated cobalamin using the ground-state structure are in good agreement with measured ground-state XANES spectrum. The difference between the calculated ground- and excited-state structures is in good qualitative and quantitative agreement with the isotropic difference spectrum measured at 1.5 ps (Figure 7a). The only adjustable parameters in Figure 7 are the Fermi energy (7.7145 keV) and the percent excitation (~20%). This agreement provides direct experimental support for the theoretically predicted structure.

The x and $y + z$ contributions to the difference spectrum are compared with the simulation in Figure 7b. The relative magnitude of x and $y + z$ signals at 1.5 ps are accurately predicted by simulation. To a first approximation, excitation results in a shift of the z-polarized XANES to lower energy, giving a derivative-like difference spectrum. This shift reflects the well-known $\sim 1/R^2$ dependence of XANES energies.[41,42] In the simulations, the x- and y-polarized difference spectra are similar and both are small, which is expected if the corrin ligation to the cobalt is similar in the ground and excited states. The agreement between the experimental and calculated x-polarized difference spectra in Figure 7b supports the assignment of x to the direction defined by the methylene groups, as indicated in Figure 1. The increased absorption at 7.7325 keV is predicted for x but not for y (see also Figure 4b).

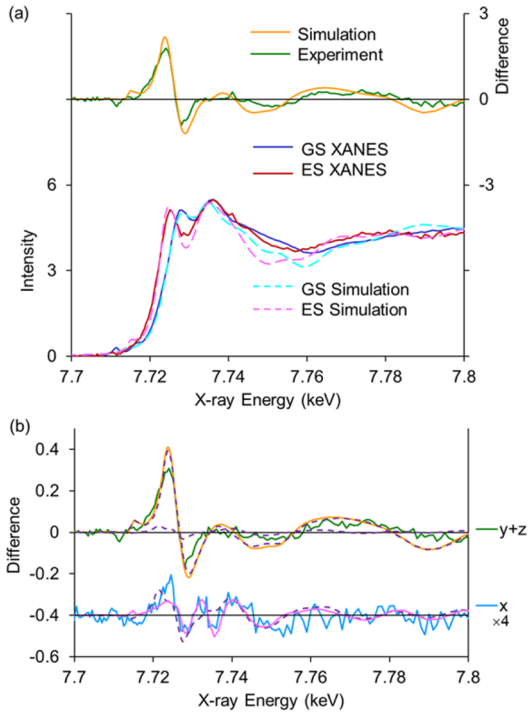

Figure 7. Comparison of experimental and simulated XANES spectra at 1.5 ps. (a) Comparison of the isotropic XANES ground- and excited-state spectra and the difference spectrum between the ground and excited state. The measurement provides the ground-state spectrum (blue) and the difference spectrum (green). The estimated excited-state spectrum (red) is calculated by adding the appropriate percentage of the ground-state spectrum into the measured difference spectrum (see Supporting Information for details). (b) Components x, y, and z of the difference spectrum are compared. The $y + z$ difference (green) is plotted on the left-hand scale. The x difference (blue) is multiplied by 4 and offset for clarity. The $y + z$ simulation (yellow) is decomposed into the y and z contributions (violet dashed lines), with z making the largest contribution. The y contribution (violet dashed line) is also compared with the simulated x (pink) contribution.

CONCLUSIONS

The picture emerging from the data starts with formation of the Franck−Condon excited state on a time scale that is not distinguished from the instrumental limit determined by the convolution of the pump and probe pulses. This is followed by internal conversion to the $(\pi^1(\sigma^*d_{z^2})^1)$ intermediate accompanied by rapid elongation of the axial bonds on a ca. 110 fs time scale. Corrin ring relaxation in the excited state follows on a ca. 260 fs time scale. Within the noise level of this measurement, there is no evidence for structural changes on a longer time scale. Internal conversion to the ground state occurs on a 6.2 ps time scale. Although the same time constants are observed in UV−visible transient absorption data, it is only with the polarized XANES measurement that it is possible to assign these time constants to specific structural changes.

Time-resolved polarized XAS provides a powerful tool for unraveling structural transformations in isotropic systems. The results reported here exploit the in-plane polarization of the lowest absorption band of CNCbl. This allows direct separation of the axial and equatorial dynamics around the central cobalt in the observed XANES difference spectra. Simulations provide additional insights. These observations reveal features that influence the reactivity, stability, and deactivation of electronically excited cobalamins. Ultrafast polarized XANES will be applicable to any system where it is possible to identify a well-defined molecular excitation direction.

ASSOCIATED CONTENT

Supporting Information

The Supporting Information is available free of charge on the ACS Publications website at DOI: 10.1021/jacs.6b11295.

Detailed description of XANES experimental methods, UV−visible transient absorption methods and analysis, detailed analysis of time-resolved XANES data, methods for simulation of XANES ground- and excited-state spectra, and sample input files for the XANES simulations (PDF)

DOI: 10.1021/jacs.6b11295
J. Am. Chem. Soc. 2017, 139, 1894−1899

AUTHOR INFORMATION

Corresponding Author

*rsension@umich.edu

ORCID

Kevin J. Kubarych: 0000-0003-1152-4734

Roseanne J. Sension: 0000-0001-6758-0132

Notes

The authors declare no competing financial interest.

[¶]Visiting Professor.

ACKNOWLEDGMENTS

This work was supported by grants from the National Science Foundation NSF-CHE 1150660 and NSF-CHE 1464584 to R.J.S. and NSF-CHE 1300239 to K.J.K. Use of the Linac Coherent Light Source (LCLS), SLAC National Accelerator Laboratory, is supported by the U.S. Department of Energy, Office of Science, Office of Basic Energy Sciences under Contract No. DE-AC02-76SF00515.

REFERENCES

(1) Rury, A. S.; Wiley, T. E.; Sension, R. J. *Acc. Chem. Res.* **2015**, *48*, 860−867.

(2) Jost, M.; Simpson, J. H.; Drennan, C. L. *Biochemistry* **2015**, *54*, 3231−3234.

(3) Jost, M.; Fernandez-Zapata, J.; Polanco, M. C.; Ortiz-Guerrero, J. M.; Chen, P. Y. T.; Kang, G.; Padmanabhan, S.; Elias-Arnanz, M.; Drennan, C. L. *Nature* **2015**, *526*, 536−U167.

(4) Kutta, R. J.; Hardman, S. J. O.; Johannissen, L. O.; Bellina, B.; Messiha, H. L.; Ortiz-Guerrero, J. M.; Elias-Arnanz, M.; Padmanabhan, S.; Barran, P.; Scrutton, N. S.; Jones, A. R. *Nat. Commun.* **2015**, *6*, 7907.

(5) Gruber, K.; Krautler, B. *Angew. Chem., Int. Ed.* **2016**, *55*, 5638−5640.

(6) Shell, T. A.; Lawrence, D. S. *Acc. Chem. Res.* **2015**, *48*, 2866−2874.

(7) Cammarata, M.; Bertoni, R.; Lorenc, M.; Cailleau, H.; Di Matteo, S.; Mauriac, C.; Matar, S. F.; Lemke, H.; Chollet, M.; Ravy, S.; Laulhe, C.; Letard, J. F.; Collet, E. *Phys. Rev. Lett.* **2014**, *113*, 227402.

(8) Lemke, H. T.; Bressler, C.; Chen, L. X.; Fritz, D. M.; Gaffney, K. J.; Galler, A.; Gawelda, W.; Haldrup, K.; Hartsock, R. W.; Ihee, H.; Kim, J.; Kim, K. H.; Lee, J. H.; Nielsen, M. M.; Stickrath, A. B.; Zhang, W. K.; Zhu, D. L.; Cammarata, M. *J. Phys. Chem. A* **2013**, *117*, 735−740.

(9) Shelby, M. L.; Lestrange, P. J.; Jackson, N. E.; Haldrup, K.; Mara, M. W.; Stickrath, A. B.; Zhu, D.; Lemke, H. T.; Chollet, M.; Hoffman, B. M.; Li, X.; Chen, L. X. *J. Am. Chem. Soc.* **2016**, *138*, 8752−8764.

(10) Levantino, M.; Lemke, H. T.; Schiro, G.; Glownia, M.; Cupane, A.; Cammarata, M. *Struct. Dyn.* **2015**, *2*, 041713.

(11) Silatani, M.; Lima, F. A.; Penfold, T. J.; Rittmann, J.; Reinhard, M. E.; Rittmann-Frank, H. M.; Borca, C.; Grolimund, D.; Milne, C. J.; Chergui, M. *Proc. Natl. Acad. Sci. U. S. A.* **2015**, *112*, 12922−12927.

(12) Miller, N. A.; Wiley, T. E.; Spears, K. G.; Ruetz, M.; Kieninger, C.; Kräutler, B.; Sension, R. J. *J. Am. Chem. Soc.* **2016**, *138*, 14250−14256.

(13) Kozlowski, P. M.; Garabato, B. D.; Lodowski, P.; Jaworska, M. *Dalton Trans.* **2016**, *45*, 4457−4470.

(14) Lodowski, P.; Jaworska, M.; Andruniów, T.; Garabato, B. D.; Kozlowski, P. M. *Phys. Chem. Chem. Phys.* **2014**, *16*, 18675−18679.

(15) Giannotti, C. In *B12*; Dolphin, D., Ed.; John Wiley & Sons: New York, 1982; Vol. *1*, pp 393−430.

(16) Pratt, J. M. *Inorganic Chemistry of Vitamin B_{12}*; Academic Press: New York, 1972.

(17) Fugate, R. D.; Chin, C.-A.; Song, P.-S. *Biochim. Biophys. Acta, Gen. Subj.* **1976**, *421*, 1−11.

(18) Solheim, H.; Kornobis, K.; Ruud, K.; Kozlowski, P. M. *J. Phys. Chem. B* **2011**, *115*, 737−748.

(19) Lodowski, P.; Jaworska, M.; Kornobis, K.; Andruniow, T.; Kozlowski, P. M. *J. Phys. Chem. B* **2011**, *115*, 13304−13319.

(20) Kornobis, K.; Kumar, N.; Wong, B. M.; Lodowski, P.; Jaworska, M.; Andruniow, T.; Ruud, K.; Kozlowski, P. M. *J. Phys. Chem. A* **2011**, *115*, 1280−1292.

(21) Chollet, M.; Alonso-Mori, R.; Cammarata, M.; Damiani, D.; Defever, J.; Delor, J. T.; Feng, Y. P.; Glownia, J. M.; Langton, J. B.; Nelson, S.; Ramsey, K.; Robert, A.; Sikorski, M.; Song, S.; Stefanescu, D.; Srinivasan, V.; Zhu, D. L.; Lemke, H. T.; Fritz, D. M. *J. Synchrotron Radiat.* **2015**, *22*, 503−507.

(22) Minitti, M. P.; Robinson, J. S.; Coffee, R. N.; Edstrom, S.; Gilevich, S.; Glownia, J. M.; Granados, E.; Hering, P.; Hoffmann, M. C.; Miahnahri, A.; Milathianaki, D.; Polzin, W.; Ratner, D.; Tavella, F.; Vetter, S.; Welch, M.; White, W. E.; Fry, A. R. *J. Synchrotron Radiat.* **2015**, *22*, 526−531.

(23) Champloy, F.; Gruber, K.; Jogl, G.; Kratky, C. *J. Synchrotron Radiat.* **2000**, *7*, 267−273.

(24) Wiley, T. E.; Miller, W. R.; Miller, N. A.; Sension, R. J.; Lodowski, P.; Jaworska, M.; Kozlowski, P. M. *J. Phys. Chem. Lett.* **2016**, *7*, 143−147.

(25) Walker, L. A., II; Shiang, J. J.; Anderson, N. A.; Pullen, S. H.; Sension, R. J. *J. Am. Chem. Soc.* **1998**, *120*, 7286−7292.

(26) Fleming, G. R. *Chemical Applications of Ultrafast Spectroscopy*; Oxford University Press: Oxford, UK, 1986.

(27) Wiley, T. E.; Arruda, B. C.; Miller, N. A.; Lenard, M.; Sension, R. J. *Chin. Chem. Lett.* **2015**, *26*, 439−443.

(28) Harris, D. A.; Stickrath, A. B.; Carroll, E. C.; Sension, R. J. *J. Am. Chem. Soc.* **2007**, *129*, 7578−7585.

(29) Shiang, J. J.; Cole, A. G.; Sension, R. J.; Hang, K.; Weng, Y.; Trommel, J. S.; Marzilli, L. G.; Lian, T. *J. Am. Chem. Soc.* **2006**, *128*, 801−808.

(30) Jones, A. R.; Russell, H. J.; Greetham, G. M.; Towrie, M.; Hay, S.; Scrutton, N. S. *J. Phys. Chem. A* **2012**, *116*, 5586−5594.

(31) Lodowski, P.; Jaworska, M.; Andruniow, T.; Garabato, B. D.; Kozlowski, P. M. *J. Phys. Chem. A* **2014**, *118*, 11718−11734.

(32) Sension, R. J.; Harris, D. A.; Stickrath, A.; Cole, A. G.; Fox, C. C.; Marsh, E. N. G. *J. Phys. Chem. B* **2005**, *109*, 18146−18152.

(33) Sension, R. J.; Harris, D. A.; Cole, A. G. *J. Phys. Chem. B* **2005**, *109*, 21954−21962.

(34) Sension, R. J.; Cole, A. G.; Harris, A. D.; Fox, C. C.; Woodbury, N. W.; Lin, S.; Marsh, E. N. G. *J. Am. Chem. Soc.* **2004**, *126*, 1598−1599.

(35) Cole, A. G.; Yoder, L. M.; Shiang, J. J.; Anderson, N. A.; Walker, L. A., II; Banaszak Holl, M. M.; Sension, R. J. *J. Am. Chem. Soc.* **2002**, *124*, 434−441.

(36) Yoder, L. M.; Cole, A. G.; Walker, L. A., II; Sension, R. J. *J. Phys. Chem. B* **2001**, *105*, 12180−12188.

(37) Joly, Y. *Phys. Rev. B: Condens. Matter Mater. Phys.* **2001**, *63*, 125120.

(38) Bunau, O.; Joly, Y. *J. Phys.: Condens. Matter* **2009**, *21*, 345501.

(39) Brouder, C. *J. Phys.: Condens. Matter* **1990**, *2*, 701−738.

(40) Kas, J. J.; Jorissen, K.; Rehr, J. J. In *X-ray Absorption and X-ray Emission Spectroscopy*; John Wiley & Sons, Ltd.: Chichester, UK, 2016; pp 51−72.

(41) Lytle, F. W.; Greegor, R. B.; Panson, A. J. *Phys. Rev. B: Condens. Matter Mater. Phys.* **1988**, *37*, 1550−1562.

(42) Bianconi, A.; Fritsch, E.; Calas, G.; Petiau, J. *Phys. Rev. B: Condens. Matter Mater. Phys.* **1985**, *32*, 4292−4295.

DOI: 10.1021/jacs.6b11295
J. Am. Chem. Soc. 2017, 139, 1894−1899